The Eurasia Proceedings of Science, Technology, Engineering & Mathematics (EPSTEM)
ISSN: 2602-3199

The Eurasia Proceedings of Science, Technology, Engineering & Mathematics (EPSTEM), 2024

Volume 29, Pages 92-105

ICRETS 2024: International Conference on Research in Engineering, Technology and Science

Synthesis and Evaluation of an Innovative Biochar Nanocomposite Adsorbent Derived from *Cycas Revoluta* Seeds, with Potential Applications in the Removal of Cationic Dyes

Elif Gezginci
Konya Technical University

Erol Pehlivan
Konya Technical University

Abstract: In this study, novel and functional adsorbents were synthesized by using *Cycas revoluta* seed (CS) biomass. The biomass was subjected to a slow pyrolysis process at a final temperature of 500°C with a heating rate of 10°C/min to synthesize *Cycas revoluta* seed biochar (CSB). After the thermochemical conversion of biomass into biochar, the nanocomposite structure (ZrO_2NP@CSB) was synthesized by adding 5% zirconium oxide (ZrO_2) nanoparticles into biochar to increase the adsorption capacity. The synthesized adsorbents (CS, CSB, and ZrO_2NP@CSB) were characterized by XRD, FTIR, SEM, and EDX. The adsorption efficiency of these three adsorbents was investigated to remove Malachite Green (MG) and Methylene Blue (MB) dye from an aqueous solution. According to the results obtained from the adsorption experiments of the nanocomposite structure, solution pH had a significant effect on the process and the highest adsorption efficiencies were achieved at pH 9. The optimum adsorbent dose was 0.5 g/L. The process reached an equilibrium after 45 minutes and 90 minutes for MG and MB, respectively. The relevant data were in good agreement with the pseudo-second-order kinetic model. The maximum adsorbent capacities were 129.87 and 117.93 mg/g for MG and MB, respectively. The adsorption mechanism follows a monolayer Langmuir isotherm model. Experiments were carried out at different temperatures (25, 35, 45°C) to determine the effect of temperature on adsorption, and dye removal efficiency slightly increased with temperature. When repeated batch adsorption experiments were compared for raw biomass, biochar, and biochar nanocomposite adsorbents, it was observed that the raw adsorbent had a lower adsorption capacity than the biochar adsorbent. It was found that the biochar nanocomposite had the highest adsorption capacity among these three adsorbents. The findings suggest that ZrO_2NP@CSB composite is a promising, cost-effective, and functional material for water treatment and can be employed as an alternative adsorbent for removing dyes.

Keywords: Adsorption, Biochar, Nanocomposite, Water treatment

Introduction

With the increasing population and industrial growth, various industrial products are simplifying human life while simultaneously causing significant environmental destruction. Industrial processes and domestic usage result in numerous pollutants being introduced into the air, water, and soil. Water, covering three-quarters of the Earth's surface, is crucial for the ecosystem. The contamination of water with pollutants from various sources during the environmental cycle leads to significant pollution, adversely affecting human health and natural life (Rathi et al., 2021; Erkmen et al., 2019).

One type of industrial pollution is dye pollution, particularly resulting from textile industry activities. With the advancement of the textile and dye industries, numerous new synthetic dyes are being synthesized. The variety

of dyes and the large volumes of dyed water discharged during dyeing processes make this type of wastewater a prime candidate for treatment. Dye-contaminated waters prevent sunlight from reaching aquatic environments, leading to ecological damage (Yaseen & Scholz, 2019; Erkuş et al., 2018). Due to the toxic and stable nature of components like azo, phthalocyanine, indigo, sulfur, and nitro in dye molecules, they pose significant environmental and health risks even at low concentrations. These risks vary with the type and dose of the dye, potentially causing allergic reactions, skin irritation, carcinogenic, and mutagenic effects (Pilatin & Kunduhoğlu, 2013; Robinson et al., 2001).

Treatment of such polluted water is necessary to reduce dye contamination and improve the quality of contaminated water. However, the resistant and diverse structures of dye molecules make standard treatment processes inadequate for effective dye removal (Dindar, 2019). Hence, advanced treatment methods such as adsorption, membrane filtration, ion exchange, and reverse osmosis are necessary for removing toxic dyes from aqueous environments.

Among advanced treatment methods, adsorption is a popular method due to its adjustable process conditions and high removal efficiency. Because of the high cost of adsorbents and the volume of wastewater that needs to be treated, researchers have recently been looking for affordable adsorbents. Biomass materials offer a potential adsorbent for the elimination of dye pollution since they are affordable, easily obtainable, and harmless to the environment (Parlayıcı & Pehlivan, 2021).

Biomass and Biochar as Adsorbent

Biomass refers to all biological materials derived from living or recently dead plant wastes that are not fossilized. For instance, plant seeds, roots, leaves, bark, agricultural waste, and animal waste are biomass. Utilizing waste biomass as an adsorbent is important not only for its low cost but also for recycling waste materials. Numerous studies in literature report the use of different biomass materials as adsorbents (Gayathiri et al., 2022; Ranjusha et al., 2010; Shelke et al., 2022). These studies indicate that the adsorption efficiency of biomass is often insufficient for the removal of toxic dyes. To enhance adsorption efficiency, additional processes such as surface modification or chemical activation are often applied to biomass (İmdat, 2014; Erdoğan, 2017;) (Tasmakıran, 2010). By synthesizing biochar from biomass using various methods, surface properties can be altered to make it a more suitable material for adsorption.

Biochar, meaning bio-based carbonaceous materials, has gained research interest over the past decade for its potential as an adsorbent in wastewater treatment. Due to the porous surfaces of biochars, they have a large surface area, which is advantageous for surface-based processes like adsorption. Studies have shown successful treatment of wastewater containing toxic dyes using biochar adsorbents (Baig et al., 2014; Parlayıcı & Pehlivan, 2023). The high adsorption capacity of biochar in these studies indicates effective treatment (Bayram et al., 2022; Bayram et al., 2023).

Enhancing Adsorption Efficiency with Biochar Nanocomposites

Although biochar-based adsorbents show potential for removing dye molecules from wastewater, it is not always possible to completely remove dyes due to the saturation of surface pores and the depletion of functional groups over time. One approach to solving this problem is to create composites by adding nanoparticles to charcoal adsorbents. This approach is expected to enhance the surface area of biochar and provide a synergistic effect from the composite components, leading to improved dye removal performance compared to each component alone (Rajput et al., 2022). While biomass and biochar adsorbents offer potential solutions for dye removal from wastewater, there is a need to further enhance their efficiency. The synthesis of biochar nanocomposites presents a promising strategy for achieving higher adsorption capacities and more effective wastewater treatment.

In this study, one of the dyes removed from the aqueous environment is MB. MB, a cationic dye with the chemical formula $C_{16}H_{18}ClN_3S{\cdot}3H_2O$, is commonly used for dyeing silk, cotton, and wood. Exposure to MB at a dosage of 2 mg/kg body weight can cause minor skin/eye irritation and stomach cramps, while exposure to doses greater than 47.0 mg/kg can lead to abnormal blood pressure, cardiac arrhythmias, coronary vasoconstriction, chromosomal damage, and lung toxicity (Altıntaş Yıldırım et al., 2022). The other dye removed is MG. The chemical formula of MG is $C_{23}H_{25}N_2Cl$. It is also known as benzaldehyde green because it is derived from benzaldehyde and dimethylaniline. It is used in the industry for dyeing silk, wool, leather, and

cotton (Sun et al., 2008). A study investigating the toxic effects of MG on mice found that exposure to a dose of 13.75 mg/kg body weight for 60 days resulted in increased oxidative stress, changes in brain chemicals, and altered behavior of cellular complexes. This dye causes severe eye irritation and corneal damage in humans (Biswas et al., 2021).

Cycas revoluta, commonly known as the sago palm, was selected as the raw material for adsorbent synthesis. Our objective is to recycle a natural resource by using this abundant biomass. Biochar adsorbent was produced from biomass using the slow pyrolysis method. Zirconium oxide nanoparticles were incorporated into the biochar adsorbents, resulting in a new and functional adsorbent. The biomass, biochar, and biochar nanocomposites were characterized using various methods, and their adsorption behaviors were investigated through batch adsorption experiments. Parameters affecting adsorption, such as pH, adsorbent dosage, contact time, initial dye concentration, and temperature, were studied. Based on the experimental results, optimal conditions for each adsorbent were determined. The adsorption process was examined for its conformity to Langmuir, Freundlich, and Temkin isotherm models. Kinetic and thermodynamic calculations were performed to elucidate the mechanism of the adsorption process.

Method

Materials

All chemicals were of analytical grade, and they were used as received with no further purifications. *Cycas revoluta* seeds (CS) were collected from Antalya/Manavgat region of Türkiye. MB and MG dyes were purchased from Acros Organics (New Jersey, USA). Zirconium oxide nanopowder (ZrO_2, ≤100 nm) was purchased from Sigma Aldrich (Darmstadt, Germany). Hydrogen chloride (HCl, 37%), sodium hydroxide (NaOH, 97%), and absolute ethanol (C_2H_5OH) were purchased from Merck. Deionized water (DI) from a Millipore water purification system was used in the experiments.

Production of Adsorbents

CS biomass was washed several times with DI to remove surface impurities and then dried in an oven at 70°C for 24 hours. The biomass was ground into a powder by using a laboratory-scale grinder for the adsorption experiments. The slow pyrolysis method was used for the thermochemical conversion of biomass into biochar. For this process, 20 grams of CS biomass was placed into a pyrolysis reactor made of steel material, which has high thermal resistance. The reactor was then placed in a muffin furnace and subjected to pyrolysis at a 500°C final temperature, 10°C/min heating rate, and 30 minutes of residence time at the final temperature.

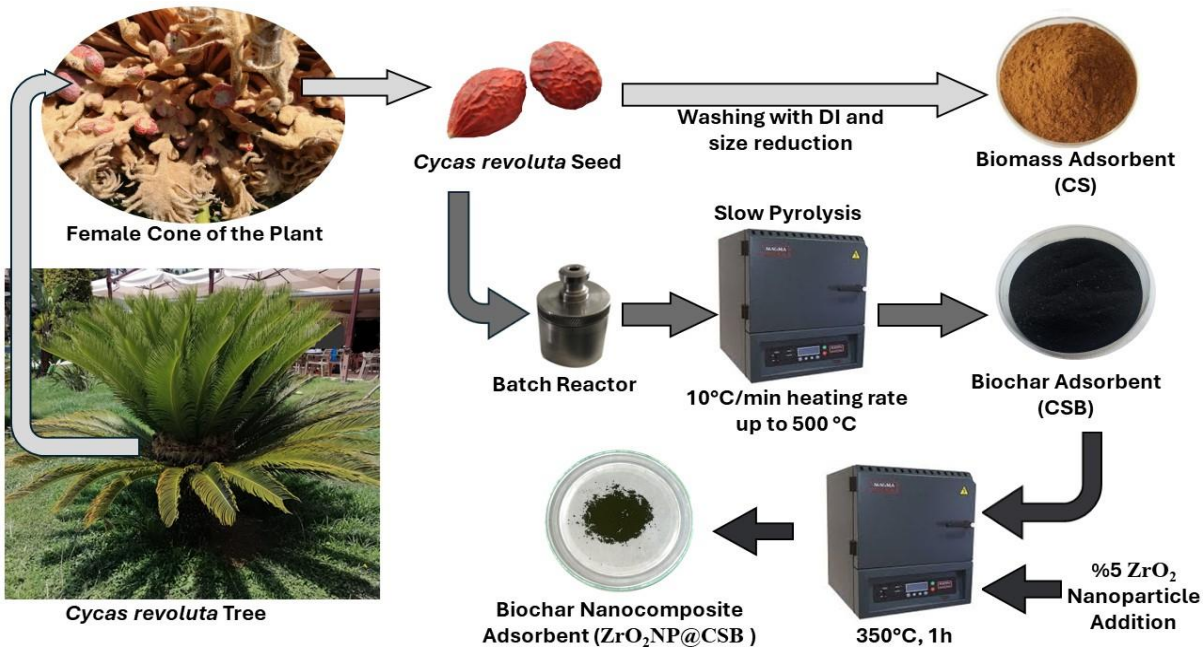

Figure 1. Schematic representation of the production steps of the CS, CSB, and ZrO_2NP@CSB

The pyrolysis product was cooled to room temperature at the same rate. At the end of the pyrolysis process, *Cycas revoluta* seed biochar (CSB) was ground into a powder with an agate mortar. Black biochar powder was obtained and stored in a sterile bottle for the analyses. The biochar nanocomposite (ZrO_2NP@CSB) was fabricated by mixing the conventionally purchased ZrO_2 nanoparticles and CSB in a %5 ratio by mass, crushed together, and treated at 350°C for 1 hour. The synthesis steps of the biomass (CS), biochar (CSB), and biochar nanocomposite (ZrO_2NP@CSB) adsorbents are illustrated in Figure 1.

Characterization Study

A ZEISS Gemini SEM 500 model scanning electron microscope (SEM) was used in order to investigate the surface morphology of the adsorbents. Energy dispersed X-ray (EDX) analyses were performed with the same device in Necmettin Erbakan University BITAM Laboratory. Before the SEM and EDX analyses, solid samples were coated with Iridium to a thickness of 4.31 nm. The presence of functional groups on the surface of the biomass, biochar, and biochar nanocomposite adsorbents was clarified by using a Thermo Scientific-Nicolet IS20 model Fourier transform infrared (FT-IR) spectrometer. FT-IR spectra were recorded within the range of 400-4000 cm^{-1}. The phase analysis of the obtained samples was investigated by the EUROPE GNR model X-ray diffraction (XRD) system with Cu-K α radiation at the $10° \leq 2\theta \leq 80°$ boundary values. The XRD spectra were recorded with an energy step size of 0.1 eV. In order to calculate the initial and final concentration of the dye solutions, the absorption spectra of the samples were obtained using a Cary 5000 UV-Vis spectrophotometer.

Batch Adsorption Experiments

The removal of MB and MG dyes was performed using synthesized adsorbents. In the batch adsorption experiments, parameters affecting adsorption such as pH, adsorbent dosage, contact time, initial concentration of dye, and temperature were investigated and optimized. The adsorption percentage was calculated by using Equation (1) and the adsorption potential per unit mass of the adsorbent, q_e (mg g^{-1}) was calculated by Equation (2).

$$\% \text{ Adsorption} = \frac{C_i - C_f}{C_i} \times 100 \quad \textbf{(1)}$$

$$q_e = \frac{(C_i - C_f)}{m} \times V \quad \textbf{(2)}$$

Where, C_i and C_f are the initial and final concentrations of the dye, respectively. V (L) is the volume of the solution and m (g) being the amount of the adsorbent. Adsorption equilibrium curves were plotted considering Langmuir, Freundlich, and Temkin isotherms. The linear Langmuir, Freundlich, and Temkin isotherm equations are given below as Equations (3), (4), and (5), respectively.

$$\frac{C_f}{q_e} = \frac{C_f}{q_m} + \frac{1}{q_m K_L} \quad \textbf{(3)}$$

$$log\, q_e = log\, K_f + \frac{1}{n} log\, C_e \quad \textbf{(4)}$$

$$q_e = B_T ln K_T + B_T ln C_e \quad \textbf{(5)}$$

Where q_m (mg g^{-1}) is the maximum adsorption capacity, K_L is the Langmuir constant, K_f is the relative sorption capacity, n is the Freundlich constant, K_T and B_T are the Temkin constants (Temkin, 1940). The calculations for adsorption kinetics were examined by comparing pseudo-first and pseudo-second-order kinetic models by using Equations (6) and (7).

$$ln(q_e - q_t) = ln\, q_e - \mathrm{t}\, k_1 \quad \textbf{(6)}$$

$$\frac{t}{q_t} = \left(\frac{1}{k_2 q_e^2}\right) + \left(\frac{1}{q_e}\right) t \quad \textbf{(7)}$$

Where q_t is the adsorption capacity at a certain time, q_e is the adsorption capacity at equilibrium, k_1 and k_2 are the pseudo-first and pseudo-second order rate constants, respectively. Thermodynamic analyses of the adsorption process were performed based on experiments which carried out at different temperatures.

Results and Discussion

Characterization Results

Figure 2. shows the FT-IR spectrum of the adsorbents. The spectrum of the CS biomass has a board band around 3400 cm^{-1}, representing the stretching of the O-H bond (Różyło et al., 2022). The intense double peaks observed at 2900 cm^{-1} and 2850 cm^{-1} are due to asymmetric and symmetric stretches from the aliphatic CH_2 group. The peak observed at 1741 cm^{-1} is a specific peak resulting from C=O stretching. This peak may originate from aldehydes, ketones, free esters, or carboxylic acids found in the pectin fibers expected in the biomass structure. The presence of a strong and narrow C=O peak with the OH and CH stretches confirms the presence of a carboxyl group in the biomass structure (Bounaas et al., 2021). The intense peak observed at 1630-1640 cm^{-1} indicates the presence of C=C and it is thought to be derived from lignin found in the palisade cells of the biomass seed (Volli et al., 2021). The peaks around 1440 cm^{-1} are due to the OH bending, and those around 1369 cm^{-1} are due to $-CH_2$ and $-CH_3$ bending. The intense peak observed at 1020-1000 cm^{-1} is the stretching vibration peak of the C-O bond.

Some of the peaks observed at the FT-IR spectrum of the biomass are absent in the biochar and biochar nanocomposite structure. As a result of a successful pyrolysis process, it is clear that large hydrocarbon groups have left the structure and that the structure has undergone carbonization. The peaks observed in the spectrum of the biochar structure (CSB) in the range of 600 to 900 cm^{-1} after pyrolysis are due to the vibrations of C-H bonds in the aromatic and heteroaromatic compounds (Hossain et al., 2011). The moderately intense peaks observed around 1580-1600 cm^{-1} in the spectrum of CSB correspond to the aromatic C=C ring in the graphite structure (Chen et al, 2008). The peak at 1395 cm^{-1} observed in the CSB sample is due to the stretching of the -C=O bond in the -COOH functional group on the biochar surface (Hassaan et al., 2023). The peaks at 489, 579, and 747 cm^{-1} observed in the spectrum of the biochar nanocomposite sample but not in the spectrum of the CSB, confirm the successful incorporation of ZrO_2 nanoparticles into the structure (Li et al., 2023).

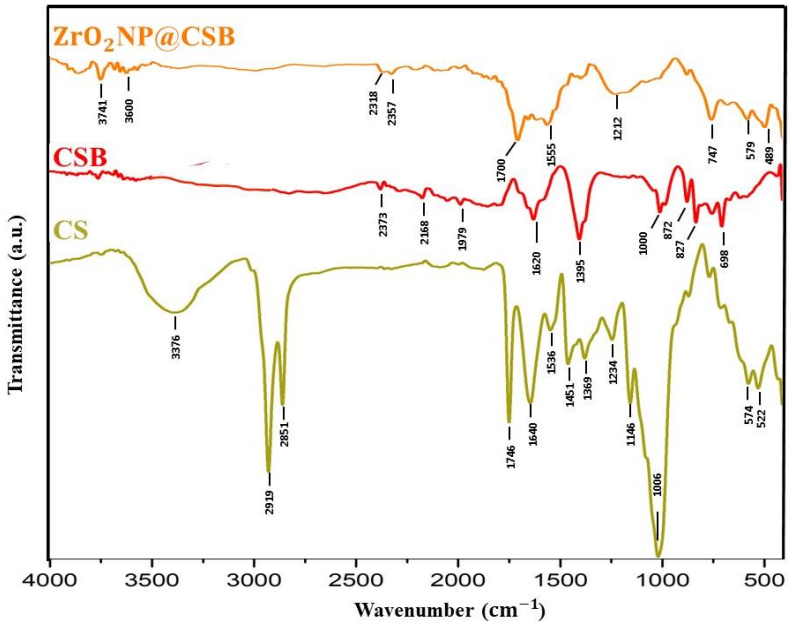

Figure 2. The FT-IR spectra of the adsorbents.

XRD analyses were conducted to reveal the structural differences between biomass, biochar, and biochar nanocomposite samples. Figure 3 shows the diffraction patterns of CS, CSB, and ZrO_2NP@CSB. The diffraction pattern of the CS biomass is characterized by a major peak at 20-23°, which is attributed to the crystalline cellulose present in the biomass (Nanda et al., 2013). In the biochar sample, a typical peak for

amorphous silica was observed at 2θ = 23° (Zeidabadi et al., 2018). The sharp peak at 30° is associated with the crystalline phase. In the XRD pattern of the biochar nanocomposite sample ZrO_2NP@CSB, the observation of the characteristic peaks for ZrO_2 at 2θ = 30.5 and 50.2 indicates that ZrO_2 nanoparticles have been successfully incorporated into the biochar matrix (Alagarsamy et al., 2022).

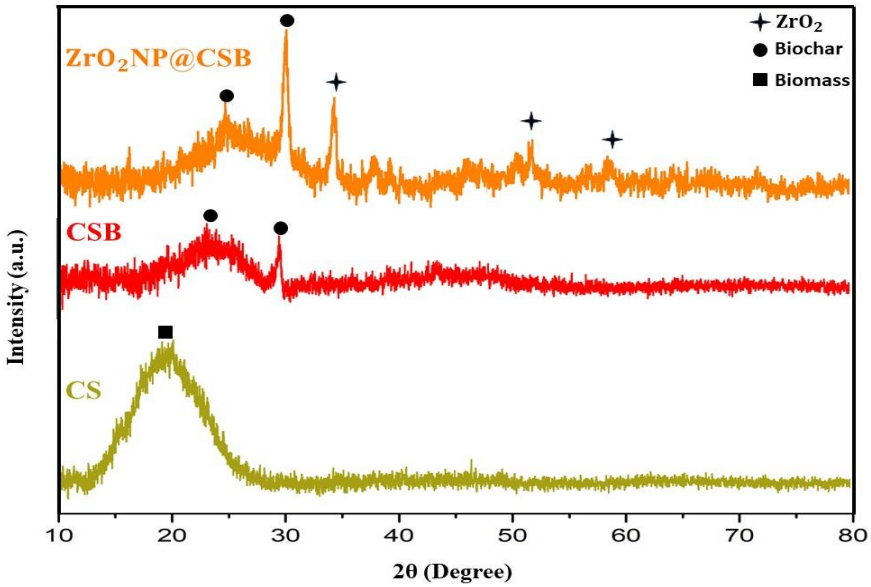

Figure 3. The XRD patterns of the adsorbents.

Figure 4 shows the SEM images of the synthesized adsorbents. According to the images, biomass sample CS has a non-pores structure. Pyrolysis is a process aimed at increasing the specific surface area by enhancing surface porosity. An increased surface area will enhance the effectiveness of surface-based processes such as adsorption, leading to more successful removal of dyes. A porous structure has been observed in the CSB. The biochar surface has circular pores of varying diameters, with sizes ranging between 0.5- 1.0 µm. The SEM image of the biochar nanocomposite ZrO_2NP@CSB reveals that the nanoparticles have been successfully incorporated into the biochar matrix. It has been found that the imbedded nanoparticles are sometimes located at the surface and inside the pores. When SEM results are evaluated regarding surface porosity, the biochar is expected to exhibit better adsorption properties than the raw biomass. The ZrO_2NP@CSB, which has metal oxide nanoparticles incorporated into the biochar matrix, is expected to demonstrate the highest adsorption capacity due to both its surface porosity and the effect of the nanoparticles on the surface area.

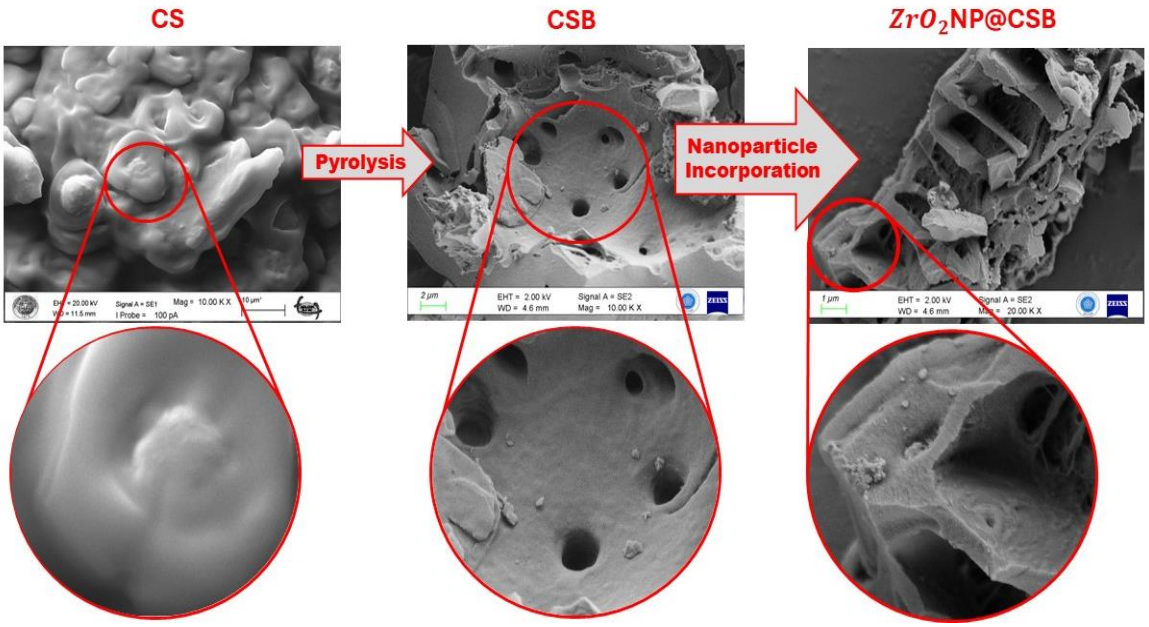

Figure 4. The SEM images of the adsorbents.

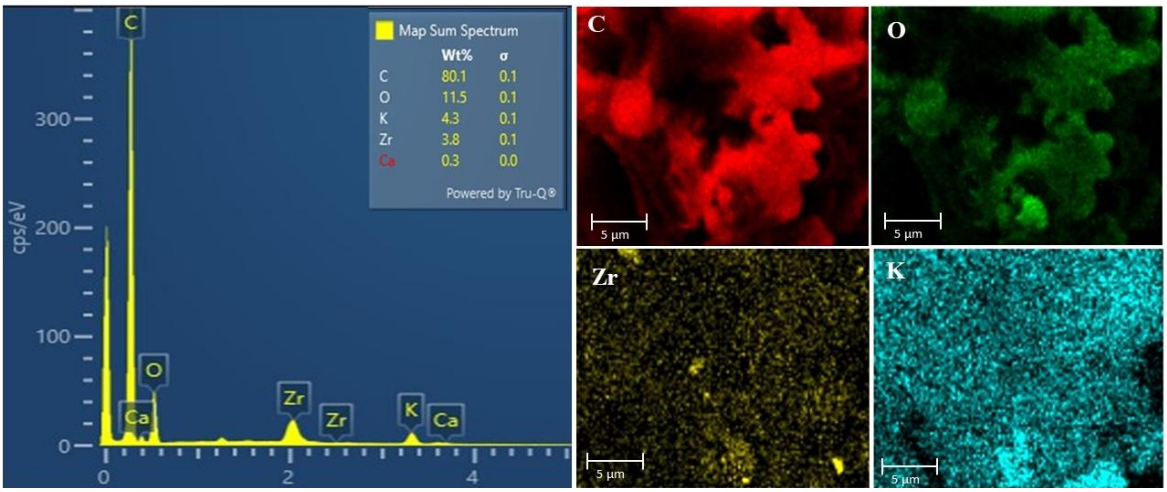

Figure 5. The EDX results of the ZrO_2NP@CSB and elemental mapping.

Using EDX analysis, the forms, distribution, and characteristics of the nanoparticles in the biochar nanocomposite sample were ascertained. The results are given in Figure 5. During elemental mapping, trace elements were not included in the mapping. The metal type of the nanoparticles added to the biochar is consistent with the EDX results. According to the results, the element with the highest proportion is carbon, which is an expected result for the biochar matrix. The element with the next highest proportion is oxygen. The oxygen source in the sample originates from the metal oxide nanoparticles and a certain amount of bound oxygen present within the sample itself.

Results of the Batch Adsorption Experiments

Effect of pH

During the adsorption process, the adsorbent and adsorbate interact in various ways. Functional groups and active sites on the surface of the adsorbent interact with the charges on the dye molecules. As the initial pH of the solution changes, the charge balance at these active sites also changes, significantly affecting the adsorption percentage. By keeping parameters such as adsorbent amount, temperature, and stirring speed constant, dye solutions with different pH values were prepared and allowed to interact for a sufficient amount of time.

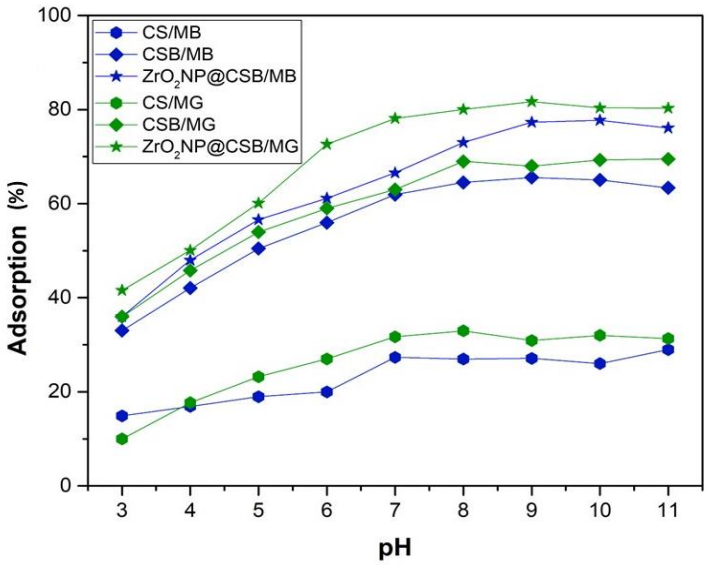

Figure 6. The effect of pH on adsorption.

At the end of the experiments, the solutions were centrifugated to separate the solid adsorbent from the dye solutions. The final concentrations of the solutions were measured by using UV-Vis. Spectrophotometer and the percentage adsorption value was calculated according to Equation (1). Figure 6 shows the effect of the initial solution pH on the adsorption % of MB and MG dyes.

According to the experimental results, the adsorption percentage of the adsorbent is low in acidic pH values, and the adsorption percentage increases as the solution pH level rises. It was observed that, for both dye removal experiments CS biomass showed maximum adsorption at pH 7, CSB at pH 8, and ZrO_2NP@CSB at 9. The better adsorption properties of the adsorbents in basic solution experiments can be explained by the occupation of limited binding sites on the adsorbent surface by H^+ ions at low pH values. The positively charged dye molecules adhere to the negatively charged adsorbent surface through an electrostatic attraction at basic pH levels. The results align with previous research findings (Altun & Ecevit, 2022).

Effect of Adsorbent Amount

The effect of the adsorbent amount on the adsorption percentage in the dye removal experiments by the synthesized adsorbents was investigated. The solution pH values were adjusted to the optimum levels determined before. In the experiments, 100 ml, 50 ppm dye solutions were prepared, and these solutions were contacted with 5 to 500 mg of adsorbents for a sufficient amount of time. The temperature was kept constant at 25°C, and the stirring speed was maintained at 400 rpm. The results obtained are presented in Figure 7.

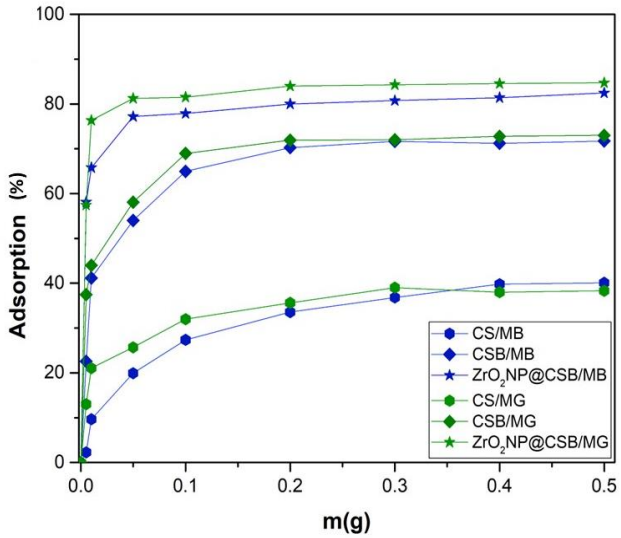

Figure 7. The effect of adsorbent amount on adsorption.

The results presented in Figure 7 can be used to evaluate the adsorption capabilities of biomass, biochar, and biochar nanocomposite adsorbents when the various amount of adsorbent used in a 100 ml, 50 ppm dye solution. The adsorption percentage increased proportionally with the increasing adsorbent dosage, up to a certain value. The adsorption percentage is only little affected by additional adsorbent additions after this point. The optimum adsorbent dosages for CS were found as 4.0 g/L and 3.0 g/L for MB and MG removal, respectively. The optimal dose of ZrO_2NP@CSB for adsorption was set at 0.5 g/L, whereas the CSB adsorbent was 2.0 g/L for both dye removal methods.

Effect of Contact Time and Kinetic Studies

Contact time is an essential factor that needs to be investigated in an equilibrium process including an adsorption study. For this purpose, 50 ppm of MB and MG solutions were mixed with a certain amount of adsorbent individually to perform adsorption. Solution pH and adsorbent amounts were adjusted to the optimum values indicated before. The adsorbent-adsorbate mixtures were allowed to interact for 1 to 240 minutes. After the specified period, the solutions were centrifuged, and a UV-Vis spectrophotometer was used to determine the solutions' ultimate concentration. The adsorption percentage versus time was plotted and presented in Figure 8. As seen in Figure 8, the adsorption of dye by the synthesized adsorbents increased rapidly for the first 0-25 minutes. After 25 minute, adsorption slowed down, and the system reached equilibrium. Adsorption does not result in appreciable variations in the adsorption % after it reaches equilibrium at a given contact time. At this equilibrium point, the active sites of the adsorbent surface are fully occupied. At 180 minutes for CS, 120 minutes for CSB, and 90 minutes for ZrO_2NP@CSB, the MB elimination process approaches equilibrium. For the MG elimination procedure, the ideal contact times were 45 minutes for ZrO_2NP@CSB, 90 minutes for CSB,

and 120 minutes for CS. Pseudo-first and pseudo-second-order equations were applied to the adsorption of MB and MG on the synthesized adsorbents and their kinetics were examined. The results are given in Table 1.

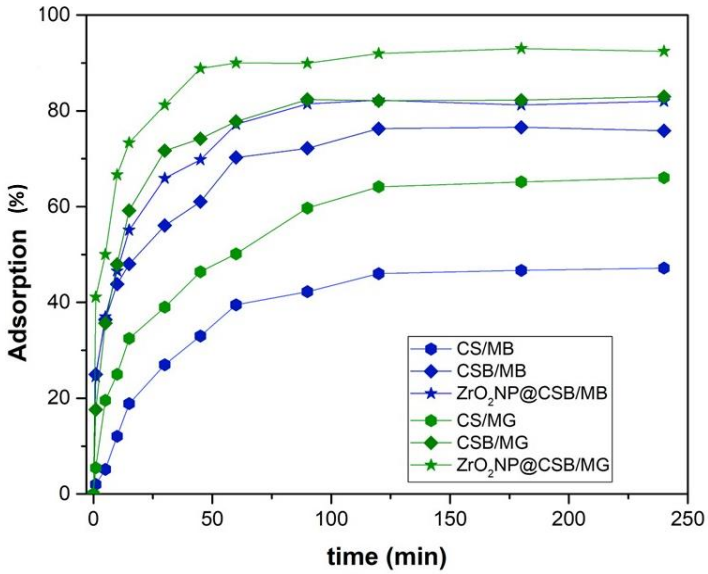

Figure 8. The effect of contact time on adsorption.

Table 1. The pseudo-first-order and pseudo-second-order parameters for the adsorption of MB and MG on CS, CSB, and ZrO_2NP@CSB

			Pseudo-first order			**Pseudo-second order**		
Adsorbent	**Dye**	$\mathbf{q_{e(exp.)}}$ **(mg/g)**	$\mathbf{R^2}$	$\mathbf{k_1}$	$\mathbf{q_e}$ **(mg/g)**	$\mathbf{R^2}$	$\mathbf{k_2}$	$\mathbf{q_e}$ **(mg/g)**
CS	MB	6.25	0.880	0.013	4.555	0.990	0.0047	6.848
CSB	MB	19.25	0.811	0.021	9.457	0.998	0.0065	19.732
ZrO_2NP@CSB	MB	82,05	0.747	0.019	34.235	0.999	0.0019	84.531
CS	MG	11.03	0.988	0.025	9.633	0.996	0.005	11.889
CSB	MG	23.02	0.619	0.009	10.444	0.999	0.008	21.322
ZrO_2NP@CSB	MG	93.50	0.770	0.019	28.539	0.999	0.003	94.192

According to Table 1, in the adsorption experiments of both dyes, the correlation coefficient for the CS biomass was calculated to be quite high in both pseudo-first-order and pseudo-second-order kinetic models (Lagergren, 1898). To determine the suitable model for this adsorbent, the experimental adsorption capacity (q_e) values were considered. It was concluded that the pseudo-second-order kinetic model is suitable for the removal of both dyes using CS. Upon evaluating the table for biochar and biochar nanocomposite, it is observed that the correlation coefficients are higher for the pseudo-second-order than the pseudo-first-order kinetic model. The experimental results also align with the pseudo-second-order kinetic model. Therefore, the pseudo-second-order kinetic model is suitable for the whole system.

Effect of Initial Concentration of Dye and Isotherm Studies

In the process of removing MB and MG dyes with synthesized adsorbents, after optimizing the parameters of pH, adsorbent dosage, and contact time, the effect of the initial concentration of dye on adsorption was investigated. During this study, experimental conditions were adjusted to the optimum conditions for each adsorbent. The initial concentration of dye was varied from 5 to 300 ppm. After reaching equilibrium, the adsorbent-dye mixtures were centrifugated, and the remaining dye concentration was measured by using UV-Vis. Spectrophotometer. Using the obtained data, isotherm graphs were plotted and presented in Figure 9. The adsorption behavior was examined within the framework of Langmuir, Freundlich, and Temkin isotherms. When examining Figure 9, it was observed that the adsorption capacity is low when the adsorbent is contacted with dyes at low concentrations, whereas it is high when the adsorbent is contacted with the dyes at high concentrations with the same amount of adsorbent. The possible reason for this is the limited number of active sites on the adsorbent's surface. When the initial concentration of dye is low, there are still active sites available for the adsorbent's surface. However, as the concentration increases, these sites gradually become occupied, and the adsorbent reaches its maximum adsorption capacity.

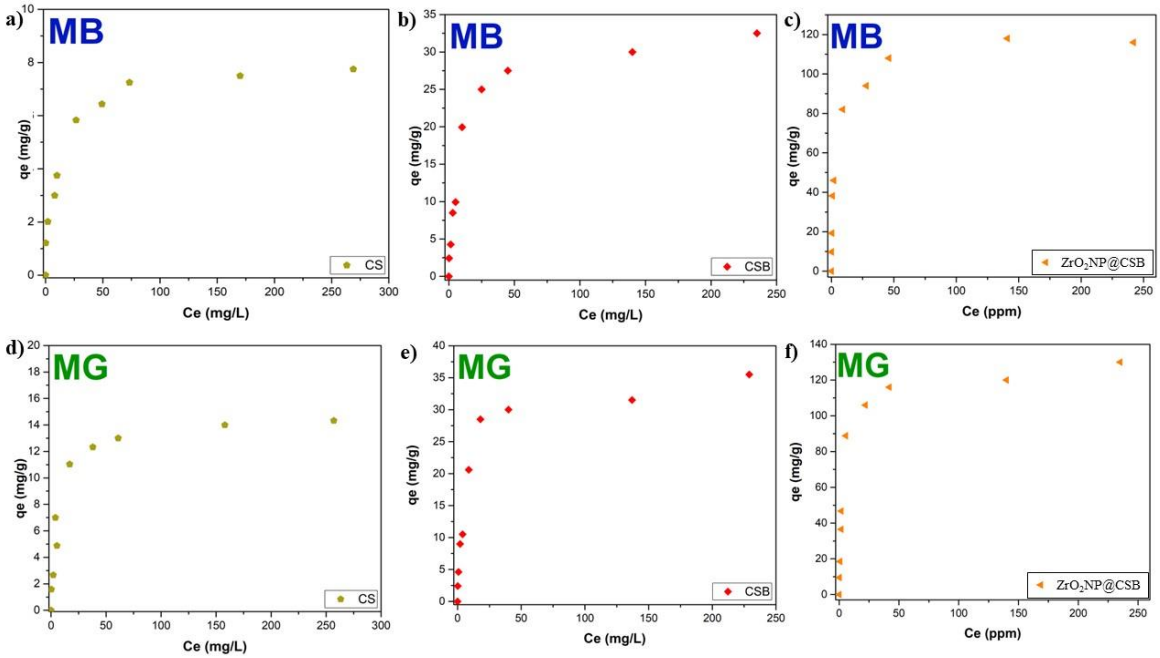

Figure 9. The effect of initial concentration of dyes on adsorption.

The plots of the graphs for the three distinct isotherms can be seen, and as the correlation coefficient R^2 gets closer to 1.0, the graph data's linearity gets better. Isotherm parameters calculated from the obtained data are presented in Table 2. Langmuir model typically describes the chemical adsorption (Langmuir, 1916). The following assumptions are made when deriving the Langmuir isotherm. (i) The surface is homogeneous. In this case, all sites on the solid surface exhibit the same adsorption properties. (ii) There are no interactions between the adsorbed molecules. Therefore, the amount of the adsorbed substance does not affect the adsorption rate per unit surface area. (iii) Adsorption is monolayer. (iv) The entire adsorption process follows the same mechanism. Similar to the Langmuir model, the equilibrium parameters are often applied to the Freundlich isotherm. According to the Freundlich model, adsorption is physical, and the adsorbent surface is heterogeneous (Freundlich, 1907). K_f and *n* parameters were calculated for the Freundlich model, if *n* values between 1 and 10, the adsorption is said to be appropriate. The Temkin isotherm assumes that the adsorption energy decreases linearly rather than exponentially as in the Freundlich.

Table 2. Parameters of Langmuir, Freundlich, and Temkin for the adsorption of MB and MG on CS, CSB, and ZrO_2NP@CSB

	Adsorbent	**Dye**	**Parameters for Dye**			
Langmuir			**q_m**	**K_L**	**R^2**	**R_L**
	CS	MB	7.930	0.114	0.998	0.149
	CS	MG	14.658	0.150	0.999	0.118
	CSB	MB	33.135	0.119	0.998	0.144
	CSB	MG	35.474	0.156	0.996	0.114
	ZrO_2NP@CSB	MB	117.925	0.326	0.999	0.058
	ZrO_2NP@CSB	MG	129.870	0.230	0.998	0.080
Freundlich			**K_f**	**n**		**R^2**
	CS	MB	1.959	3.656		0.944
	CS	MG	2.965	2.956		0.870
	CSB	MB	5.349	2.589		0.908
	CSB	MG	6.270	2.625		0.906
	ZrO_2NP@CSB	MB	29.648	3.210		0.886
	ZrO_2NP@CSB	MG	26.853	2.797		0.811
Temkin			**K_T**	**B_T**		**R^2**
	CS	MB	8.441	1.002		0.893
	CS	MG	4.798	2.146		0.906
	CSB	MB	4.026	4.781		0.901
	CSB	MG	5.816	4.738		0.930
	ZrO_2NP@CSB	MB	13.478	15.539		0.978
	ZrO_2NP@CSB	MG	6.628	19.008		0.932

When evaluating the data shared in Table 2, the correlation coefficients are closest to 1 in the Langmuir isotherm model. The fact that the distribution coefficient R_L values between 0 and 1 indicates the suitability of the Langmuir isotherm. When the R_L value is 0, adsorption is irreversible, and when it is greater than 1, the system is unfavorable for adsorption. R_L values can be calculated by using Equation (8), where K_L is the Langmuir coefficient and C_i is the initial concentration of dye.

$$R_L = \frac{1}{1+ K_L C_i} \tag{8}$$

In this study, since R_L values are between 0 and 1, it is understood that the system conforms to the Langmuir isotherm model. Although the system conforms to the Langmuir isotherm model, the correlation coefficients R^2 for the Freundlich isotherm are also quite high. It can be inferred that this model also goes along with the adsorption process because the Freundlich isotherm constant, n, supports values between 1 and 10. According to these findings, the system exhibits a structure where both physisorption and chemisorption occur simultaneously.

Effect of Temperature and Thermodynamic Studies

To determine the effect of temperature on adsorption and to perform thermodynamic calculations, experiments were conducted at 25, 35, and 45°C. During these experiments, the previously determined optimum conditions for each adsorbent were maintained. van't Hoff plots for the removal of MB and MG are provided in Figure 10.

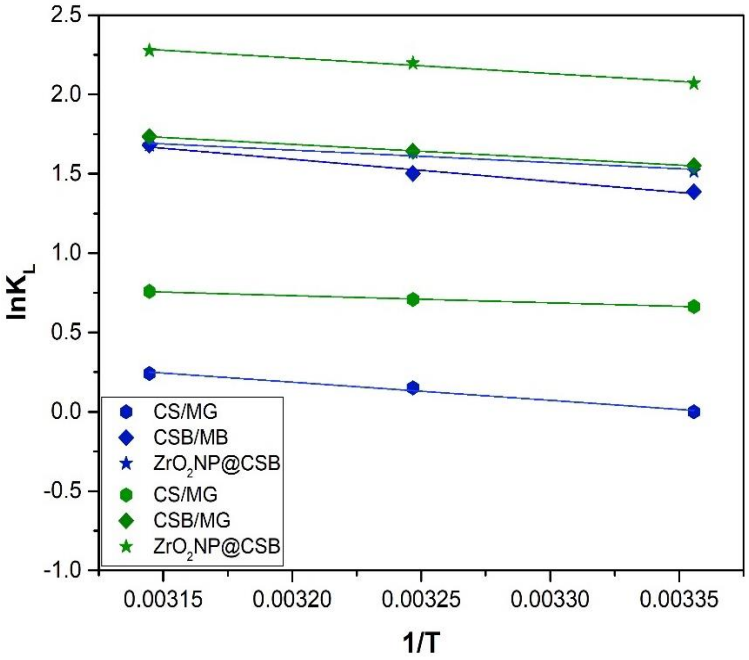

Figure 10. The van't Hoff plots of the adsorbents.

The slope and intercept values of van't Hoff plots were used to calculate the changes in entropy and enthalpy by using Equations (9) and (10). The results are presented in Table 3. Calculating thermodynamic parameters is required to ascertain whether the adsorption process is spontaneous.

$$ln\, k_e = \left(\frac{\Delta S}{R}\right) - \left(\frac{\Delta H}{R}\right)\frac{1}{T} \tag{9}$$

$$\Delta G° = \Delta H° - T\,\Delta S° \tag{10}$$

Where T is the temperature (K); R is the ideal gas constant; k_e is the equilibrium constant. From Equation (10) it is possible to calculate Gibbs free energy, $\Delta G°$ (kJ mol^{-1}). Adsorption percentage slightly increases with temperature, but this increase is not significant. Considering additional costs such as increasing the system's temperature, the optimum temperature for MB and MG adsorption with the synthesized adsorbents has been determined as 25°C.

Table 3. Thermodynamic parameters for the adsorption of MB and MG on CS, CSB, and ZrO_2NP@CSB

Dye	Adsorbent	ΔH^0 (kJ/mol)	ΔS^0 (kJ/mol.K)	ΔG^0 (kJ/mol) T= 298 K	T= 308 K	T= 318 K
MB	CS	9.52	0.032	-0.016	-0.336	-0.656
	CSB	11.57	0.050	-3.330	-3.830	-4.330
	ZrO_2NP@CSB	6.50	0.035	-3.930	-4.280	-4.630
MG	CS	3.74	0.018	-1.624	-1.804	-1.984
	CSB	7.25	0.037	-3.776	-4.146	-4.516
	ZrO_2NP@CSB	8.17	0.045	-5.240	-5.690	-6.140

The negative values of the Gibbs free energy change indicate that the adsorption process occurs spontaneously. Furthermore, the amount of the ΔG^0 suggests that physical sorption controls the process. The reaction appears to be endothermic based on the positive ΔH^0 values.

Conclusion

This study investigated the removal of MB and MG dyes from aqueous solutions by adsorbents derived from *Cycas revoluta* seed. These adsorbents are the *Cycas revoluta* seed itself, the pyrolysis product of the seed (CSB), and the nanocomposite which is synthesized by ZrO_2 nanoparticle incorporation of the *Cycas revoluta* seed biochar. Based on the SEM analyses, when comparing the surfaces of the biomass adsorbents with the biochar adsorbent, it was observed that the pyrolysis process achieved the targeted surface modification, and that the biochar possessed a porous surface. Elemental analysis revealed the presence of metal-oxide nanoparticle elements in the biochar nanocomposite adsorbents. Thus, the success of the incorporation process was confirmed. According to the experimental findings, CSB and ZrO_2NP@CSB worked best at a pH between 8.0 and 9.0 for effective dye adsorption. The pseudo-second-order kinetic model expressed the adsorption kinetic well. The adsorption of MB and MG onto the synthesized adsorbent process was fitted to the Langmuir isotherm model. The maximum adsorption capacities calculated using the Langmuir isotherm for MB removal were found to be 7.93 mg/g for CS, 33.14 mg/g for CSB, and 117.93 mg/g for ZrO_2NP@CSB. For MG removal, the maximum adsorption capacities calculated using the Langmuir isotherm were found to be 14.66 mg/g for CS, 35.47 mg/g for CSB, and 129.87 mg/g for ZrO_2NP@CSB. Comparing the adsorption efficiencies of the synthesized biomass, biochar, and biochar nanocomposite, it has been demonstrated through experiments that the biochar nanocomposite exhibited the highest adsorption efficiency. When comparing the removal of MB and MG with the same adsorbents, it was observed that MG removal achieved higher adsorption capacity with a lower equilibrium contact time and lower dosage compared to MB removal.

Scientific Ethics Declaration

The authors declare that the scientific ethical and legal responsibility of this article published in EPSTEM journal belongs to the authors.

Acknowledgements or Notes

* This article was presented as an oral presentation at the International Conference on Research in Engineering, Technology and Science (www.icrets.net) held in Tashkent/Uzbekistan on August 22-25, 2024.

* This study is derived from the Master's thesis prepared by the first author under the supervision of the second author.

References

Alagarsamy, A., Chandrasekaran, S., & Manikandan, A. (2022). Green synthesis and characterization studies of biogenic zirconium oxide (ZrO2) nanoparticles for adsorptive removal of methylene blue dye. *Journal of Molecular Structure, 1247*, 131275.

Altintas Yildirim, O., & Pehlivan, E. (2023). Removal of methylene blue using a novel generation photocatalyst based on nano-SnO2/wild plumb kernel shell biochar composite. *Journal of Dispersion Science and Technology*, *44*(14), 2748-2759.

Altun, T., & Ecevit, H. (2022). Adsorption of malachite green and methyl violet 2B by halloysite nanotube: Batch adsorption experiments and Box-Behnken experimental design. *Materials Chemistry and Physics*, *291*, 126612.

Baig, S. A., Zhu, J., Muhammad, N., Sheng, T., & Xu, X. (2014). Effect of synthesis methods on magnetic Kans grass biochar for enhanced As (III, V) adsorption from aqueous solutions. *Biomass and Bioenergy*, *71*, 299-310.

Bayram, O., Moral, E., & Göde, F. (2023). İğde çekirdeklerinden elde edilen biyokömür kullanılarak sulu çözeltiden kristal viyole boyarmaddesinin uzaklaştırılması. *Journal of the Institute of Science and Technology*, *13*(1), 448-457.

Bayram, O., Köksal, E., Moral, E., Göde, F., & Pehlivan, E. (2023). Efficient decolorization of cationic dye (malachite green) by natural-based biosorbent (nano-magnetic Sophora Japonica fruit seed biochar). *Journal of Dispersion Science and Technology*, *45*(1), 117-128.

Biswas, P., Hasan, W., Jain, J., Kori, R. K., Bose, D., & Yadav, R. S. (2022). Non-permitted food colorants induced neurotoxicity in cerebellum of rat brain. *Drug and Chemical Toxicology*, *45*(6), 2852-2859.

Bounaas, M., Bouguettoucha, A., Chebli, D., Gatica, J. M., & Vidal, H. (2021). Role of the wild carob as biosorbent and as precursor of a new high-surface-area activated carbon for the adsorption of methylene blue. *Arabian Journal for Science and Engineering*, *46*, 325-341.

Chen, B., Zhou, D., & Zhu, L. (2008). Transitional adsorption and partition of nonpolar and polar aromatic contaminants by biochars of pine needles with different pyrolytic temperatures. *Environmental Science & Technology*, *42*(14), 5137-5143.

Dindar, N. (2019). *Tekstil endüstrisi atıksularında ileri arıtma prosesleri kullanılarak organik madde giderimi*. (Master's thesis), Pamukkale Üniversitesi Fen Bilimleri Enstitüsü, Denizli-Türkiye

Erdoğan, F. O. (2017). Düşük maliyetli adsorbentler üzerine dispers sarı 211 tekstil boyasının adsorpsiyonu. *Afyon Kocatepe Üniversitesi Fen ve Mühendislik Bilimleri Dergisi*, *17*(3), 889-898.

Erkmen, J., Kavcı, E., & Adıgüzel, M. (2019). Üretim planlaması yapılarak su bazlı boyaların üretimi esnasında oluşan su kirliliğinin ve boya kaybının önlenmesi. *Journal of the Institute of Science and Technology*, *9*(1), 57-65.

Erkuş, A., Oygun, E., Türkmenoğlu, M., & Aldemir, A. (2018). Boya endüstrisi atıksularının karakterizasyonu. *Yüzüncü Yıl Üniversitesi Fen Bilimleri Enstitüsü Dergisi*, *23*(3), 308-319.

Freundlich, H., (1907). Über die adsorption in lösungen, *Zeitschrift für physikalische Chemie*, 57(1), 385-470

Gayathiri, M., Pulingam, T., Lee, K. T., & Sudesh, K. (2022). Activated carbon from biomass waste precursors: Factors affecting production and adsorption mechanism. *Chemosphere*, *294*, 133764.

Hassaan, M. A., Yılmaz, M., Helal, M., El-Nemr, M. A., Ragab, S., & El Nemr, A. (2023). Isotherm and kinetic investigations of sawdust-based biochar modified by ammonia to remove methylene blue from water. *Scientific Reports*, *13*(1), 12724.

Hossain, M. K., Strezov, V., Chan, K. Y., Ziolkowski, A., & Nelson, P. F. (2011). Influence of pyrolysis temperature on production and nutrient properties of wastewater sludge biochar. *Journal of Environmental Management*, *92*(1), 223-228.

İmdat, S. Ş., (2014). Haşhaş kabuğunun sitrik asit ile modifiye edilerek, yeni adsorban hazırlanması ve sulu çözeltilerden Cr (VI) iyonunun uzaklaştırılması, (Master's thesis), *Selçuk Üniversitesi Fen Bilimleri Enstitüsü,* Konya-Türkiye

Lagergren, S., (1898). Zur theorie der sogenannten adsorption geloster stoffe, *Kungliga Svenska Vetenskapsakademiens Handlingar*, 24, 1-39

Langmuir, I., (1916). The constitution and fundamental properties of solids and liquids. Part I: Solids, *Journal of the American Chemical Society*, *38* (11), 2221-2295

Li, X. F., Li, R. X., & Feng, X. Q. (2023). Photocatalytic Activity of Ag/AgCl/ZrO2@ Biochar Composite for Rhodamine B and Methyl Orange Dyes. *Russian Journal of Physical Chemistry A*, *97*(4), 633-646.

Nanda, S., Mohanty, P., Pant, K. K., Naik, S., Kozinski, J. A., & Dalai, A. K. (2013). Characterization of North American lignocellulosic biomass and biochars in terms of their candidacy for alternate renewable fuels. *Bioenergy Research*, *6*, 663-677.

Parlayıcı, Ş., & Pehlivan, E. (2021). Biosorption of methylene blue and malachite green on biodegradable magnetic Cortaderia selloana flower spikes: modeling and equilibrium study. *International Journal of Phytoremediation*, *23*(1), 26-40.

Parlayıcı, Ş., & Pehlivan, E. (2023). An ecologically sustainable specific method using new magnetic alginate-biochar from acorn cups (Quercus coccifera L.) for decolorization of dyes. *Polymer Bulletin*, *80*(10), 11167-11191.

Pilatin, S., & Kunduhoğlu, B. (2013). Phanerochaete chrysosporium tarafından bazı reaktif tekstil boyalarının renk giderimi ve detoksifikasyonu. *Biological Diversity and Conservation*, *6*(3), 26-34.

Rajput, V. D., Minkina, T., Ahmed, B., Singh, V. K., Mandzhieva, S., Sushkova, S., ... & Wang, B. (2022). Nano-biochar: A novel solution for sustainable agriculture and environmental remediation. *Environmental Research*, *210*, 112891.

Ranjusha, V. P., Pundir, R., Kumar, K., Dastidar, M. G., & Sreekrishnan, T. R. (2010). Biosorption of Remazol Black B dye (Azo dye) by the growing Aspergillus flavus. *Journal of Environmental Science and Health Part A*, *45*(10), 1256-1263.

Rathi, B. S., Kumar, P. S., & Vo, D. V. N. (2021). Critical review on hazardous pollutants in water environment: Occurrence, monitoring, fate, removal technologies and risk assessment. *Science of the Total Environment*, *797*, 149134.

Robinson, T., McMullan, G., Marchant, R., & Nigam, P. (2001). Remediation of dyes in textile effluent: a critical review on current treatment technologies with a proposed alternative. *Bioresource Technology*, *77*(3), 247-255.

Różyło, K., Jędruchniewicz, K., Krasucka, P., Biszczak, W., & Oleszczuk, P. (2022). Physicochemical characteristics of biochar from waste cricket chitin (Acheta domesticus). *Molecules*, *27*(22), 8071.

Shelke, B. N., Jopale, M. K., & Kategaonkar, A. H. (2022). Exploration of biomass waste as low cost adsorbents for removal of methylene blue dye: A review. *Journal of the Indian Chemical Society*, *99*(7), 100530.

Sun, X. F., Wang, S. G., Liu, X. W., Gong, W. X., Bao, N., Gao, B. Y., & Zhang, H. Y. (2008). Biosorption of Malachite Green from aqueous solutions onto aerobic granules: Kinetic and equilibrium studies. *Bioresource Technology*, *99*(9), 3475-3483.

Tasmakıran, A. F., (2010). *Zirai yan ürünlerin modifiye edilerek yeni adsorbanların hazırlanması ve boyaların adsorpsiyonu*, (Master's thesis), Selçuk Üniversitesi Fen Bilimleri Enstitüsü, Konya-Türkiye

Temkin, M., (1940). Kinetics of ammonia synthesis on promoted iron catalysts, *Acta Physiochim*, 12, 327-356

Yaseen, D. A., & Scholz, M. (2019). Textile dye wastewater characteristics and constituents of synthetic effluents: a critical review. *International journal of Environmental Science and Technology*, *16*, 1193-1226.

Volli, V., Gollakota, A. R. K., & Shu, C. M. (2021). Comparative studies on thermochemical behavior and kinetics of lignocellulosic biomass residues using TG-FTIR and Py-GC/MS. *Science of the Total Environment*, *792*, 148392.

Zeidabadi, Z. A., Bakhtiari, S., Abbaslou, H., & Ghanizadeh, A. R. (2018). Synthesis, characterization and evaluation of biochar from agricultural waste biomass for use in building materials. *Construction and Building Materials*, *181*, 301-308.

Author Information

Elif Gezginci
Konya Technical University, Faculty of Engineering and Natural Sciences, Department of Chemical Engineering
Rauf Orbay Street. 42250, Selçuklu/Konya, Türkiye

Erol Pehlivan
Konya Technical University, Faculty of Engineering and Natural Sciences, Department of Chemical Engineering
Rauf Orbay Street. 42250, Selçuklu/Konya
Contact e-mail: *erolpehlivan@gmail.com*

To cite this article:

Gezginci, E. & Pehlivan, E. (2024). Synthesis and evaluation of an innovative biochar nanocomposite adsorbent derived from *Cycas revoluta* seeds, with potential applications in the removal of cationic dyes. *The Eurasia Proceedings of Science, Technology, Engineering & Mathematics (EPSTEM), 29*, 92-105.